Research Square

Preprints are preliminary reports that have not undergone peer review.
They should not be considered conclusive, used to inform clinical practice,
or referenced by the media as validated information.

The lncRNA Brip1os Orchestrates IFN-γ–Mediated Inflammatory-Myogenic Crosstalk to Promote Muscle Regeneration

Yi Luo
Third Affiliated Hospital of Sun Yat-sen University
Jia-Dong Zhang
Third Affiliated Hospital of Sun Yat-sen University
Wei-Cai Chen
Third Affiliated Hospital of Sun Yat-sen University
Wan-Xin Chen
Third Affiliated Hospital of Sun Yat-sen University
Zhi-Xuan Zhang
Third Affiliated Hospital of Sun Yat-sen University
Ya-Rui Hou
Third Affiliated Hospital of Sun Yat-sen University
Pan-Long Li
Third Affiliated Hospital of Sun Yat-sen University
Xiao-Fen Zhong
Third Affiliated Hospital of Sun Yat-sen University
Zhen-Dong Xiao
Third Affiliated Hospital of Sun Yat-sen University
Jie-Hua He
Sun Yat-sen Memorial Hospital
Li-Ting Diao
Third Affiliated Hospital of Sun Yat-sen University
Qi Zhang
Third Affiliated Hospital of Sun Yat-sen University
Shu-Juan Xie
xieshj5@mail.sysu.edu.cn

Third Affiliated Hospital of Sun Yat-sen University

Article

Keywords:

Posted Date: June 12th, 2026

DOI: https://doi.org/10.21203/rs.3.rs-9886579/v1

License: This work is licensed under a Creative Commons Attribution 4.0 International License.
Read Full License

Additional Declarations: No competing interests reported.

Abstract

Skeletal muscle regeneration is a highly choreographed process governed by the dynamic interplay between myogenic progenitors and the inflammatory microenvironment. However, the molecules that integrate early inflammatory signals with myogenic fate transitions remain poorly understood. Here, we identify the long noncoding RNA (lncRNA) *Brip1os* as a critical sentinel that orchestrates this crosstalk. *Brip1os* expression is inversely correlated with postnatal skeletal muscle development but is robustly and specifically induced during the early inflammatory phase following muscle acute injury. Functional assays demonstrate that *Brip1os* sustains the myogenic proliferative pool by promoting myoblast expansion and preventing premature differentiation. Mechanistically, we show that *Brip1os* regulates a set of IFN-γ-responsive genes and is continuously upregulated in injured muscle cells during the early phase through a positive feedback loop involving M1 macrophages. Notably, loss of *Brip1os* in vivo leads to a breakdown of this inflammatory-myogenic crosstalk, manifested by impaired M1 macrophage recruitment and defective muscle repair, and exogenous IFN-γ supplementation partially rescues regeneration in *Brip1os*-deficient mice. Collectively, our findings reveal a *Brip1os*-mediated regulatory hub that tunes the early inflammatory response to support effective tissue repair, offering a promising therapeutic target for regenerative failure and muscle wasting disorders.

Introduction

Skeletal muscle regeneration is a multifaceted and highly coordinated process that is essential for restoring tissue integrity and functional competence following injury or pathological insult. This regenerative potential is predominantly reliant on a resident population of stem cell, namely satellite cells or muscle stem cells (MuSCs) [1]. Upon injury, quiescent satellite cells undergo activation, proliferation, and subsequently differentiation into form new myofibers, or undergo self-renew to replenish the stem cell pool [2–4]. The successful execution of these sequential events is orchestrated by a complex crosstalk between intrinsic myogenic programs and extrinsic signals from the dynamic injury microenvironment [5]. Among these external signals, the early inflammatory phase, characterized by the infiltration of immune cells such as macrophages, exerts a critical and dualistic regulatory role. It is well established that during the early phase of acute injury, immune cells including natural killer (NK) cells and effector T cells are among the initial responders, secreting substantial quantities of interferon-gamma (IFN-γ) [6,7], which drives the polarization of naïve (M0) macrophages into the pro-inflammatory M1 phenotypes [8,9]. These M1 macrophages function to phagocytose cellular debris, thereby mitigating persistent inflammation and secondary damage, and in turn establishing a permissive microenvironment for subsequent tissue regeneration [10]. Concomitantly, M1 macrophages can suppress the expression of pro-fibrotic factors such as transforming growth factor-beta 1 (TGF-β1), attenuating scar tissue formation and thus contributing to efficient repair processes [11–13]. Despite the well-documented roles of myogenic transcription factors and specific cytokines, the regulatory networks that integrate these inflammatory signals with MuSC fate determination during this critical early stage, particularly those involving long non-coding RNAs (lncRNAs), remain incompletely elucidated.

LncRNAs, defined as transcripts longer than 200 nucleotides with limited protein-coding potential, have emerged as key regulators of gene expression in diverse biological contexts, including muscle physiology and pathology [14]. Recent studies highlight their central roles in skeletal muscle development, homeostasis, and the pathogenesis of various muscle disorders. For instance, MEG3 promotes the liquid – liquid phase separation of SUZ12, stabilizes the PRC2 complex, and represses downstream target genes such as Fhl3 and Rnf128, thereby regulating muscle fiber type specification, mitochondrial function, and lipid metabolism [15]. In facioscapulohumeral muscular dystrophy (FSHD), FRG2 binds to repetitive sequences (including rDNA), suppressing ribosomal RNA transcription and protein synthesis, which in turn leads to impaired muscle-specific protein production [16]. Furthermore, the dysregulation of lncRNAs in the muscle of cancer patients underscores their potential as both biomarkers and mediators of muscle dysfunction in systemic diseases [17], cementing their crucial role in muscle homeostasis. Despite these advances, however, their specific functions in acute muscle injury and regeneration, particularly in mediating the critical crosstalk between the early inflammatory microenvironment and muscle stem cell fate reprogramming, remain a significant knowledge gap.

Previous studies from our laboratory have reported that lncRNA *Brip1os* is significantly downregulated during myoblast differentiation [18], while its functional role remained to be fully elucidated. In the current study, we confirmed lncRNA *Brip1os* is specifically induced during the early phase of skeletal muscle injury. Functional analysis demonstrated that *Brip1os* promotes myoblast proliferation while suppressing their differentiation. Mechanistically, interferon-gamma (IFN-γ), a key inflammatory cytokine derived from the early injury microenvironment, was identified as a critical upstream inducer of *Brip1os*. Previous studies have established that appropriate levels of IFN-γ are essential for normal skeletal muscle repair following injury in the early stage. During early regeneration, IFN-γ transiently inhibits myogenic differentiation via specific pathways, such as CIITA activation, thereby helping to maintain muscle stem cells in a proliferative state to facilitate subsequent effective regeneration [19,20]. Our study further reveals that *Brip1os* regulates a set of IFN-γ-responsive genes, and may also drive macrophage polarization toward the M1 phenotype by modulating IFN-γ secretion, thereby achieving a pro-regenerative effect. These M1 macrophages subsequently amplify *Brip1os* expression in skeletal muscle through intercellular communication, establishing a positive feedback loop. Notably, *Brip1os* is indispensable for efficient muscle regeneration in vivo. In the absence of *Brip1os*, M1 macrophage polarization is impaired, injury repair is suppressed, and supplementation with IFN-γ partially rescues the inhibition of injury repair. Collectively, this study identifies *Brip1os* as a central molecular node that integrates early inflammatory signals with myogenic cell fate determination, providing a new perspective for understanding the immune–stem cell crosstalk during skeletal muscle regeneration.

Results

Brip1os Is Downregulated During Myogenic Differentiation but Specifically Activated During the Early Phase of Skeletal Muscle Injury Repair.

Our preliminary RNA sequencing (RNA-seq) analysis identified a set of lncRNAs that were both highly expressed (mean FPKM > 1) and significantly dysregulated during the differentiation of C2C12 myoblasts (at day 4 post-differentiation) (Fig. S1a) [18]. To validate this, we examined *Brip1os* expression in a C2C12 myoblast differentiation model spanning the growth medium (GM) phase and days 2, 4, and 6 post-differentiation (D2, D4, D6) (Fig. S1b). The results confirmed that *Brip1os* expression was progressively downregulated (Fig. S1c), accompanied by a robust increase in both the mRNA and protein levels of the myogenic differentiation markers MyHC and MEF2C (Fig. S1d-e). To further investigate the role of *Brip1os* in physiological myogenesis, we assessed its expression levels in mouse skeletal muscle at key embryonic and postnatal time points. The results showed a progressive downregulation of *Brip1os* expression throughout development (Fig. 1a). To confirm this trend at the cellular level, we isolated primary myoblasts from 4- to 5-week-old mice (Fig. 1b). Flow cytometry analysis indicated that cells cultured for 48h post-isolation contained a high proportion of muscle stem cells with good viability (Fig. S2a). During *in vitro* induced differentiation (GM phase and days 0, 1, and 2 of differentiation [DM] culture) (Fig. S2b), we also observed a progressive downregulation of *Brip1os* expression as differentiation progressed, with its level at day 2 (D2) reduced to 40% of that in the GM phase (Fig. 1c). Concurrently, the expression of myosin heavy chain (MyHC) and MEF2C was significantly upregulated (Fig. S2c-d). These highly concordant findings from both *in vivo* developmental and *in vitro* differentiation models demonstrate that *Brip1os* expression is negatively correlated with the myogenic process, suggesting its potential role as a negative regulator of myoblast differentiation.

Notably, *Brip1os* displayed a distinct expression pattern during pathological regeneration. To explore its function in skeletal muscle repair following injury, we established an acute injury model by intramuscular injection of cardiotoxin (CTX) into the tibialis anterior (TA) muscle of mice. Hematoxylin and eosin (H&E) staining confirmed that the TA muscle tissue exhibited typical post-injury changes, including necrosis, inflammatory cell infiltration, and subsequent regeneration (Fig. 1d). Analysis of RNA-seq data from TA muscle tissues at 1, 3, and 5 days post-injury (dpi) from our previous study (Fig. 1e, S2e) [21] revealed that, among numerous differentially expressed lncRNAs (mean FPKM > 1), *Brip1os* was the most significant upregulation on 3 dpi compared with 1 and 5 dpi, reaching 6.87-fold increase. This result was independently validated by quantitative real-time PCR (qPCR), which confirmed that the *Brip1os* transcriptional levels peaked on 3 dpi (Fig. 1f, g). Consistently, the expression levels of the proliferation marker Ki67 and the MuSC marker PAX7 in TA muscle tissue was also significantly elevated on 3 dpi (Fig. 1h-i), coinciding with the active phase of regenerative repair. Collectively, these findings demonstrate a context-dependent dual expression pattern of *Brip1os*. It is downregulated during physiological myogenesis but specifically activated in the early phase of skeletal muscle injury repair, indicating that *Brip1os* may play a critical and complex role in regulating myogenic cell fate and skeletal muscle regeneration.

Brip1os Promotes Myoblast Proliferation and Inhibits Terminal Myogenic Differentiation.

To investigate the functional role of *Brip1os* in myoblast biology, we established a stable *Brip1os* overexpression model in C2C12 myoblasts. qPCR analysis confirmed a 13.6-fold upregulation of *Brip1os*

transcript levels in overexpression cells relative to control cells (Fig. 2a). Under proliferative conditions (growth medium, GM), Western blot (WB) and immunofluorescence (IF) staining revealed that *Brip1os* overexpression significantly increased the protein levels of PAX7 and Ki67 (Fig. 2b, c, S3a). This pro-proliferative phenotype was further validated by crystal violet colony formation assays (Fig. 2d) and Cell Counting Kit-8 (CCK-8) proliferation assays (Fig. 2e), both of which demonstrated that *Brip1os* overexpression enhanced cell proliferative capacity and clonogenic potential.

Following in vitro induction of myogenic differentiation for three days (day 3, D3), *Brip1os*-overexpressing C2C12 cells exhibited markedly reduced MyHC expression compared to empty vector-transfected control cells (Fig. 2f, g, S3a). Quantitative analysis of differentiation parameters further revealed that *Brip1os* overexpression led to a significant decrease in both the percentage of MyHC-positive cells and the number of multinucleated myotubes (Fig. 2g). Collectively, these findings indicate that *Brip1os* is sufficient to promote myoblast proliferation while concurrently suppressing terminal myogenic differentiation.

Knockdown of Brip1os Inhibits Myoblast Proliferation and Promotes Myogenic Differentiation.

To confirm the functional necessity of *Brip1os* in myoblast biology, we performed loss-of-function studies by knocking down *Brip1os* expression in C2C12 myoblasts. qPCR validation showed that two independent dCas9-knockdown cell lines achieved knockdown efficiencies of approximately 89% and 85%, respectively, relative to the control (Fig. 3a). Under proliferative conditions (GM culture), *Brip1os* knockdown significantly reduced the protein levels of PAX7 and Ki67 (Fig. 3b, c, S3b). Crystal violet colony formation assays (Fig. 3d) and CCK-8 proliferation assays (Fig. 3e) further confirmed that *Brip1os* depletion impaired myoblast proliferative capacity and clonogenic potential. Conversely, following induction of myogenic differentiation in vitro, *Brip1os*-knockdown cells exhibited a marked enhancement in MyHC expression (Fig. 3f, g, S3b). Quantitative analysis of differentiation parameters clearly demonstrated that *Brip1os* knockdown led to a significant increase in both the percentage of MyHC-positive cells and the number of multinucleated myotubes (Fig. 3g). Taken together, these phenotypes, which are opposite to those observed in the overexpression experiments, demonstrate that *Brip1os* is required for maintaining myoblasts in a proliferative state and for preventing premature myogenic differentiation.

Brip1os Regulates a Panel of IFN-γ-Responsive Genes and Is Co-activated With Early M1 Macrophage Infiltration Following Injury.

To further elucidate the molecular mechanism by which *Brip1os* mediates muscle injury repair, we first performed RNA sequencing to analyze transcriptomic changes in C2C12 myoblasts following *Brip1os* knockdown. Differential expression analysis of the sequencing data revealed 297 overlapping genes among all identified differentially expressed genes (Fig. 4a). Further analysis of significantly changed genes ($p.adj < 0.05$) identified 18 overlapping genes in the two knockdown samples (Fig. 4b), 6 of which were IFN-γ-responsive genes, suggesting a potential role for *Brip1os* in regulating the IFN-γ-related signaling network (Fig. 4c). The expression trends of these downstream genes were confirmed in

independent *Brip1os*-knockdown C2C12 cell lines (Fig. S4a). To further characterize the signaling pathways and biological processes regulated by *Brip1os*, we performed KEGG and GO enrichment analyses on both transcriptomic (RNA-seq) and proteomic datasets.

First, KEGG pathway analysis of the RNA-seq data revealed that *Brip1os*-regulated genes were significantly enriched in the RIG-I-like receptor and NOD-like receptor signaling pathways (Fig. 4d). Both pathways are core components of the innate immune system responsible for inducing interferon production. Consistently, GO biological process enrichment analysis of the same dataset showed that the differentially expressed genes were predominantly involved in antiviral immunity and interferon responses (Fig. 4e). These results indicate that *Brip1os* knockdown markedly affects the expression of genes linked to interferon signaling and innate immune responses, suggesting that *Brip1os* plays an important role in regulating IFN-γ-mediated immune reactions.

To validate these findings at the protein level, we performed proteomic analysis on the same *Brip1os*-knockdown cell line (KD-1). KEGG pathway enrichment analysis of the proteomic data revealed that differentially expressed proteins were significantly enriched in pathways related to cell adhesion, migration, and survival, including “focal adhesion”, “ECM-receptor interaction”, and the “PI3K-Akt signaling pathway” (Fig. 4f). Furthermore, GO biological process analysis showed that these proteins are primarily involved in “actin cytoskeleton organization”, “collagen fibril organization”, and “cellular response to type II interferon (IFN-γ)” (Fig. 4g). Taken together, the transcriptomic and proteomic data are highly consistent, collectively indicating that *Brip1os* may regulate myoblast proliferation and differentiation by modulating cytoskeletal remodeling, extracellular matrix interactions, and IFN-γ signaling responses.

Thus, the RNA-seq and proteomic results convergently demonstrate that the gene set regulated by *Brip1os* is enriched in interferon-responsive genes. To clarify the cellular basis of *Brip1os*-mediated genes regulation, we analyzed its subcellular localization by subcellular fractionation assays (Fig. S4b), found that *Brip1os* is predominantly enriched in the cytoplasm (Fig. S4c), since IFN-γ response genes mainly located in cytoplasm, we further suppose that *Brip1os* exerts its pro-proliferative effect by regulating IFN-γ secretion.

Brip1os Co-activates with M1 Infiltration and Downstream Genes in the Early Stage of Skeletal Muscle Injury.

Given that IFN-γ induces M1 macrophages during the early stage of tissue injury, and that M1 macrophages exert a pro-repair effect in the early stage of skeletal muscle injury repair [5], we therefore simultaneously examined the expression of downstream genes and the infiltration of M1 macrophages during the injury process in subsequent experiments. Firstly, we examined the TA at 3 days post-injury (3 dpi) in the CTX-induced model (Fig. 5a). Immunofluorescence staining revealed a significant increase in M1 macrophage ($F4/80^{+}CD86^{+}$) infiltration at the injury site (Fig. 5b), consistent with previous studies. Furthermore, analysis of six IFN-γ-responsive genes in the injured TA muscle tissue showed that all genes were coordinately upregulated at the transcriptional level at 3 dpi (Fig. 5c). These *in vivo* results

indicate that *Brip1os*, M1 macrophage infiltration, and the downstream IFN-γ-responsive gene network are synergistically activated during the early phase of skeletal muscle injury.

Subsequently, to verify the inductive effects of IFN-γ on M1 macrophage infiltration and downstream gene expression during the early stage of skeletal muscle injury repair, we performed an *in vivo* gain-of-function experiment. After inducing injury with CTX in the bilateral TA muscles of mice, we locally injected IFN-γ into one TA muscle, while the contralateral TA muscle received saline as a control (Fig. 5d). The results showed that IFN-γ treatment, as expected, significantly enhanced local M1 macrophage infiltration (Fig. 5e), consistently upregulated the expression of *Brip1os* and all six downstream IFN-γ-responsive genes (Fig. 5f, g). These findings indicate that during the early stage of skeletal muscle injury repair, IFN-γ induces M1 macrophage infiltration and coordinately upregulates the downstream IFN-γ-responsive gene network, while *Brip1os* is concurrently activated, suggesting its potential involvement in IFN-γ-mediated early repair regulation.

In Vivo Knockdown of Brip1os Impairs Skeletal Muscle Regeneration and Attenuates the Early M1 Macrophage Response

To define the physiological function of *Brip1os* in muscle injury repair *in vivo*, we performed local *in vivo* *Brip1os* knockdown in the mouse CTX-induced TA muscle injury model (Fig. 6a), and harvested the tissues for analysis at day 3 post-injury, effective *Brip1os* silencing at the injury site was verified by qPCR (Fig. 6b, S5a). Histological analysis revealed that, compared to the contralateral NC control side, the *Brip1os*-knockdown side exhibited significant regeneration impairment at 3 dpi, characterized by disorganized myofiber architecture, impaired clearance of necrotic debris, and a significantly reduced cross-sectional area of regenerating myofibers (Fig. 6c). Immunofluorescence results also confirmed decreased infiltration of M1 macrophages ($F4/80^{+}CD86^{+}$) upon *Brip1os* knockdown (Fig. 6d), indicating that *Brip1os* is essential for effective initiation of the regenerative program.

Subsequently, Western blot and qPCR analyses showed that *Brip1os* knockdown led to significantly reduced expression levels of PAX7 and Ki67 (Figs. 6e, 6f, S5b). Furthermore, the expression levels of the previously identified downstream IFN-γ-responsive gene network, which is regulated by *Brip1os*, were also decreased in the *Brip1os* knockdown group (Fig. 6g). Collectively, these results suggest that *Brip1os* deficiency results in insufficient M1 macrophage infiltration and attenuated downstream IFN-γ signaling, thereby impairing MuSC activation and proliferation, ultimately leading to regenerative failure. This demonstrates that *Brip1os* is a critical molecule that coordinates M1 macrophage recruitment and the activation of the regenerative program during the early phase following skeletal muscle injury.

IFN-γ Treatment Partially Reversed The In Vivo Knockdown Phenotype of Brip1os.

To clarify the functional relationship between IFN-γ and *Brip1os*, we performed an in vivo IFN-γ rescue experiment in the context of *Brip1os* knockdown. After injecting CTX into the bilateral tibialis anterior (TA) muscles of mice, we injected si-*Brip1os* bilaterally on the following day, while simultaneously administering a local injection of IFN-γ into one side and saline into the contralateral side as a control.

Tissues were collected for analysis at day 3 post-injury (Fig. 7a). We found that exogenous IFN-γ as expected enhanced M1 macrophage infiltration at the injury site (Fig. 7c). Meanwhile, H&E staining confirmed that IFN-γ supplementation improved injury repair outcomes, with partial restoration of the cross-sectional area of regenerating myofibers (Fig. 7b).

Subsequently, we also examined downstream molecules. The results confirmed that IFN-γ supplementation partially upregulated the expression levels of PAX7 and Ki67 (Figs. 7d, 7e, S5c) and improved the activation of the downstream IFN-γ-responsive gene network (Fig. 7f), consistent with the aforementioned histological findings. These results suggest that the pro-regenerative effect of *Brip1os* during the early stage of skeletal muscle injury repair may be mediated through IFN-γ, which can directly activate M1 macrophage polarization and promote M1 infiltration at the injury site, thereby exerting a pro-regenerative effect.

Brip1os Regulates Bidirectional Myoblast-Macrophage Crosstalk.

Lastly, to investigate whether M1 macrophages and myoblasts interact with each other using *Brip1os* as a potential node in the injury microenvironment, we established a non-contact co-culture system. Firstly, LPS-polarized M1 macrophages were co-cultured with primary myoblasts (Fig. 8a). qPCR analysis revealed that, compared with the control group containing an empty upper chamber, co-culture with M1 macrophages for 6 hours significantly upregulated *Brip1os* expression in myoblasts (Fig. 8b), suggesting that M1 macrophages may regulate the proliferative status of myoblasts by inducing *Brip1os* to promote early post-injury skeletal muscle repair.

Interestingly, this regulation is bidirectional. In the reciprocal co-culture experiment, primary myoblasts were co-cultured with unpolarized M0 macrophages (Fig. 8c). Flow cytometry analysis showed that after 6 hours of co-culture with myoblasts, the proportion of macrophages polarized toward the M1 phenotype ($CD11b^+F4/80^+CD86^+$) was significantly higher than that in the control group with an empty upper chamber, increasing from 13.47% to 20.83% (Fig. 8d, S6a). This result indicates that myoblasts themselves can secrete signaling factors to actively shape their local immune microenvironment and promote macrophage polarization toward the pro-inflammatory M1 phenotype.

Taken together, these findings suggest the existence of a regulatory loop involving *Brip1os* within the microenvironment during the early stage of skeletal muscle injury repair. At the early phase of injury, *Brip1os* is upregulated in muscle cells at the injury site, which subsequently induces increased secretion of IFN-γ by immune cells. This IFN-γ promotes the polarization and infiltration of M1 macrophages at the injury site, creating a pro-regenerative environment through phagocytosis and secretion. Meanwhile, there is a reciprocal interaction between M1 macrophages and myoblasts: M1 macrophages directly induce *Brip1os* expression in myoblasts, promoting their proliferation and increasing the proportion of stem cells. Conversely, myoblasts also promote the polarization of M1 macrophages, thereby forming a positive feedback loop that further enhances the pro-regenerative effect. These effects ultimately manifest as upregulated expression of the proliferation marker Ki67, increased cross-sectional area of myofibers at the injury site, and improved skeletal muscle repair following injury.

Discussion

Skeletal muscle injury repair is a highly coordinated, dynamic process involving the tightly orchestrated integration of sequential stages, including inflammatory clearance, myogenic activation, and tissue remodeling [22,23]. The bidirectional crosstalk between immune cells and MuSCs in the early phase of injury is a critical determinant of repair efficiency and quality [20]. Although lncRNAs are known to play significant roles in muscle homeostasis, how they integrate early inflammatory signals with myogenic fate decisions remains a critical knowledge gap in the field [24,25].

Our study reveals the pro-regenerative function of the lncRNA *Brip1os* during the early stage of skeletal muscle injury repair. *Brip1os* is upregulated in the early phase of skeletal muscle injury, promotes myoblast proliferation and inhibits differentiation, and mediates the interaction between M1 macrophages and myoblasts. Deficiency of *Brip1os* may reduce M1 macrophage recruitment and the expression of IFN-γ-responsive genes by affecting IFN-γ secretion, leading to regenerative failure. Supplementation with IFN-γ partially reverses the regenerative inhibition induced by *Brip1os* knockdown.

Previous research on lncRNAs in muscle repair has largely focused on their cell-autonomous regulation of myogenic cells, such as modulating key genes involved in myoblast proliferation or differentiation. However, efficient skeletal muscle regeneration also critically depends on timely and spatiotemporally precise crosstalk between immune cells and myogenic cells following injury. During the early stage of injury, M1 macrophages play a central role in promoting injury repair. In addition to their phagocytic function [26,27], studies have also confirmed that their regulatory effect on muscle stem cells can be mediated by small molecules such as 11,22-EET [28]. Although the central role of macrophages in this process is well established, the specific molecular hubs linking the early inflammatory immune response to MuSC fate reprogramming-particularly the role of lncRNAs in the intercellular communication-remain poorly defined. Our experiments provide new insights into the interaction between muscle cells and immune cells during the early phase of skeletal muscle injury repair.

Notably, the regulatory role of *Brip1os* in IFN-γ signaling may have broader physiological and pathological implications. Recent studies have uncovered multiple mechanisms by which lncRNAs participate in the regulation of IFN-γ signaling. For instance, Cao *et al.* demonstrated that the lncRNA Sros1 promotes IFN-γ-mediated innate immune activation in macrophages by stabilizing Stat1 mRNA [29]. In another study, lncRNA CD244 was shown to suppress IFN-γ expression in $CD8^+$ T cells by recruiting EZH2 to the IFN-γ/TNF-α promoter region, thereby mediating H3K27 trimethylation [30]. Furthermore, Bhatt *et. al* also identified two RNA-based molecular subtypes in the skeletal muscle of patients with cancer cachexia [31]. This finding provides indirect yet compelling clinical evidence supporting the critical role of hub lncRNAs in muscle-wasting diseases, and further reinforces the clinical translational potential of *Brip1os* as a key regulator of both muscle regeneration and muscle-wasting disorders.

From a clinical translational perspective, the discovery of *Brip1os* offers a new potential target for intervening in muscle regeneration disorders, with clear therapeutic promise. First, the unique expression

pattern of *Brip1os*, which is specifically upregulated after injury, endows it with biomarker potential for assessing the efficiency of the inflammation-to-regeneration transition in early muscle injury. Consistent with this, *Brip1os* has also been identified as a key regulator and potential biomarker in macrophage foam cells in atherosclerosis [32], highlighting its broad relevance across different inflammatory pathologies. Second, accumulating evidence supports the utility of lncRNAs as biomarkers and therapeutic targets in muscle regeneration disorders. Lei *et. al* reported that lncRNA AK159072 promotes myoblast proliferation and muscle regeneration by activating the Akt/Foxo1 pathway, and knockdown of AK159072 in a CTX-induced muscle injury model significantly reduces myofiber cross-sectional area and delays regeneration, suggesting that modulating its expression may represent a potential therapeutic strategy for diseases such as muscular dystrophy and sarcopenia[33]. Similarly, Wang *et. al* found that lncRNA DLEU2 acts as a sponge for miR-181a, inhibiting skeletal muscle differentiation and regeneration by regulating SEPP1, and its expression level is closely associated with sarcopenia risk, serving as a predictive tool for this disease[34]. Furthermore, Yao *et. al* reported that lncRNA-MEG3 regulates muscle mass and metabolic homeostasis by promoting liquid-liquid phase separation of SUZ12, providing a new therapeutic avenue for muscle metabolic diseases [35]. Third, targeting the *Brip1os*-IFN-γ regulatory axis may represent a novel therapeutic strategy for correcting the regenerative microenvironment. Recently, Jin et al. successfully enhanced IFN-γ-stimulated gene transcription and cell-intrinsic anti-infective defense by developing specific antisense oligonucleotides (ASOs) targeting the interaction between lncRNA XR_001779380 and the Prdm1 protein[36], providing a strategic framework for RNA-based therapies targeting *Brip1os*-IFN-γ interactions. Collectively, these studies indicate that lncRNA-targeted therapy is moving from concept toward practice, laying a solid theoretical and strategic foundation for the clinical translation of *Brip1os*.

In summary, this study positions *Brip1os* as an indispensable molecule connecting early innate immune responses with myogenic regeneration after injury, revealing a function of lncRNAs in mediating complex intercellular communication to coordinate tissue repair. Nevertheless, several key questions remain to be explored: First, although *Brip1os* is predominantly cytoplasmic, its precise mode of molecular action remains unclear, whether it exerts its physiological effects via a competing endogenous RNA (ceRNA) mechanism, protein-protein interaction, or by modulating mRNA stability. Future work should combine RNA pull-down and mass spectrometry to identify protein interactors of *Brip1os* and elucidate how it regulates the transcription or stability of IFN-γ-responsive genes. Second, this study was based on an acute CTX-induced injury model; the expression and functional dynamics of *Brip1os* in chronic muscle-wasting diseases, such as sarcopenia, cancer cachexia, and Duchenne muscular dystrophy, are critical for determining its clinical relevance. In particular, the dysregulation of hub lncRNAs in the molecular subtypes of cancer cachexia identified by Bhatt *et al*[31], suggests that *Brip1os* may play a similarly critical role in chronic wasting conditions, warranting validation in future clinical cohort studies. Finally, in the middle and late stages of injury repair, M2 macrophages play a dominant regulatory role. In the context of fibrosis, macrophages exhibit a dysregulated and persistent mixed pro-inflammatory/pro-fibrotic phenotype, failing to undergo the orderly M1-to-M2 transition from a pro-inflammatory to a pro-repair state [37]. However, this study did not examine whether *Brip1os* deficiency affects the M1-to-M2

phenotypic switch, nor did it elucidate the role of M2 macrophages in this feedback loop, these unresolved issues point to future research directions. In summary, *Brip1os* serves as a key molecular hub linking early innate immunity with muscle regeneration, deepening our understanding of immune-stem cell crosstalk and offering a promising therapeutic target for muscle repair and related wasting disorders.

Materials and Methods

Animal Experiments

4-week-old male C57BL/6J mice were obtained from GemPharmatech Co., Ltd. (Nanjing, China) and housed under specific pathogen-free conditions with controlled temperature, humidity, and ventilation. The muscle injury model was established by intramuscular injection of cardiotoxin (CTX; Merck Micropore, 217503) into the tibialis anterior (TA) muscle. Briefly, CTX powder was dissolved in sterile saline to a 10 μM working solution. Under anesthesia, 25 μL of CTX solution was injected into the mid-belly of the unilateral or bilateral TA muscles. Control groups received an equal volume of saline.

For siRNA-mediated knockdown, in vivo-ready siRNA was purchased from GenePharma Co., Ltd. (Suzhou, China), dissolved in saline, and injected at 0.5 OD per site. For IFN-γ treatment, Recombinant IFN-γ (PeproTech, 315-05) was diluted in saline to 60 μg/mL, and 20 μL (1.2 μg) was injected per site. Animals were euthanized at designated time points post-injury (days 1, 3, 5). TA muscles were harvested, with portions flash-frozen in liquid nitrogen for molecular analysis or fixed in 4% paraformaldehyde (Servicebio, G1101) for histology. siRNA sequences are listed in Supplementary Table 1.

Hematoxylin and Eosin (H&E) Staining

Fixed muscle tissues were dehydrated through a graded ethanol series, cleared in xylene, and paraffin-embedded. Sections (5 μm) were cut, deparaffinized, rehydrated, and stained with hematoxylin and eosin following standard protocols. After dehydration and clearing, sections were mounted with neutral resin. Images were captured using a light microscope to assess myofiber morphology, necrosis, inflammation, and regeneration.

Immunofluorescence Staining of Tissue Sections

Following deparaffinization, rehydration, and antigen retrieval of paraffin-embedded tissue sections, the subsequent steps were performed similarly to the immunofluorescence staining protocol for cells (blocking, primary/secondary antibody incubation, Hoechst counterstaining). After mounting with anti-fade mounting medium, the sections were observed and images were captured using an upright fluorescence microscope or a confocal microscope.

Reverse Transcription Quantitative Real-Time PCR (RT-qPCR)

Total RNA was extracted using TRIzol reagent (Invitrogen, 15596018CN). RNA concentration and purity were measured (NanoDrop). First-strand cDNA was synthesized from 1 μg RNA using HiScript III RT SuperMix for qPCR (+ gDNA wiper) (Vazyme, R323-01). qPCR was performed with ChamQ Universal SYBR qPCR Master Mix (Vazyme, Q711-02) using a QuantStudio system. The GAPDH gene served as the internal control. Relative expression was calculated via the 2^(-ΔΔCt) method, with unpaired t-tests for comparisons. Primer sequences are listed in ed in Supplementary Table 2.

Western Blot

Total protein was extracted using RIPA lysis buffer (WSHT, EZPS03-1) containing protease inhibitor (Roche, 04693132001), phosphatase inhibitor (Roche, 04906837001), and RNase inhibitor (HaiGene, C2001B). Protein concentration was determined by BCA assay (KeyGen BioTECH, KGB2101). Equal protein amounts were separated by SDS-PAGE, transferred to PVDF membranes (Merck Millipore, IPVH00010), and blocked with 5% skim milk. Membranes were incubated with primary antibodies (Supplementary Table 3) overnight at 4°C, followed by HRP-conjugated secondary antibodies (Cell Signaling, 7074S for rabbit, 7076S for mouse). Signals were detected with chemiluminescent substrate (advansta, K-12045-D50) and visualized. GAPDH served as the loading control.

Cell Culture and Stable Cell Line Generation

Cell Culture

C2C12 cells were cultured in DMEM (Gibco, C11995500CP) supplemented with 10% fetal bovine serum (ExCell, FSP500) and 1% penicillin-streptomycin (Keygen BIO, KGL2303-100) at 37°C with 5% CO_2. To induce differentiation, growth medium was replaced with differentiation medium (DMEM with 2% horse serum (Gibco, 16050122)).

Construction of Stable Cell Lines

For the overexpression construct, the Lv201-puro-*Brip1os* plasmid was purchased from IGeneBio. The *Brip1os* overexpression sequence was inserted into the pLVX-puro vector using Gibson assembly. For the knockdown construct, a *Brip1os* gene knockdown system was established using the CRISPR-dCas9 system. Two complementary single-guide RNAs (sgRNAs) targeting the promoter region of *Brip1os* were cloned into the lentiviral vector pLV HU6-sgRNAHUBc-dCas9-KRABT2a-Puro using BsmB restriction enzyme and Gibson assembly.

Lentivirus was produced by co-transfecting HEK-293T cells with the target vector, pSPAX2 (encoding HIV-1 Gag/Pol for viral core assembly), and pMD2.G (expressing the VSV-G broad-tropism envelope glycoprotein) at a molar ratio of 4:3:1 using polyethylenimine (sigma, 919012) (PEI). Viral supernatants were collected 48 hours post-transfection, filtered through a 0.45-μm PVDF membrane, and stored at -80°C. C2C12 cells were infected with the lentiviral particles. Selection with puromycin (2 μg/mL) was initiated 24 hours post-infection and maintained for 2 days to obtain stable cell lines. All primer sequences used are listed in Supplementary Table 4.

Mouse Primary Myoblast Isolation and Culture

Briefly, Limb muscles were harvested from 4-5-week-old C57BL/6J mice, minced, and digested at 37°C for 45 minutes in a solution containing 0.2% collagenase type II (Gibco, 17101-015) and 0.1% dispase (Gibco, 17105-041). The digestion step was repeated twice. The resulting cell suspension was filtered through a 70-μm cell strainer (Biolglx, 15-1070) and centrifuged to pellet the cells. The cell pellet was resuspended in myoblast growth medium (F10 medium (Gibco, 11550-043) supplemented with 20% fetal bovine serum (Gibco, 10099141C), 1% penicillin-streptomycin (Keygen BIO, KGL2303-100), and 20 ng/mL hFGF (Abmole, M11108)). Myoblasts were purified by the differential adhesion method and subsequently seeded onto culture dishes pre-coated with 0.2% gelatin (Sigma, 9000-70-8). When cells reached 40–50% confluency, they were passaged using 0.25% trypsin (Gibco, 25200-072). To induce differentiation, the growth medium was replaced with differentiation medium (DMEM (Gibco, C11995500CP) containing 2% horse serum (Gibco, 16050122)) when cells reached 90% confluency.

Mouse Bone Marrow-Derived Macrophage Isolation and Culture

Bone marrow cells were flushed from mouse femurs and tibiae using ice-cold RPMI-1640 medium (Gibco, C11875500BT). After centrifugation, red blood cells were lysed using Red Blood Cell Lysis Buffer (Beyotime, C3702). The cells were resuspended in complete macrophage medium (RPMI-1640 medium supplemented with 10% fetal bovine serum (ExCell, FSP500), 1% penicillin-streptomycin (Keygen BIO, KGL2303-100), and 20 ng/mL M-CSF (ABclonal, RP01216)) and seeded onto culture dishes. Cells were incubated at 37°C in a 5% CO_2 atmosphere for 7 days, with a half-medium change performed every 3 days. The adherent M0 macrophages obtained were polarized towards the M1 phenotype by stimulation with 100 ng/mL LPS (Sigma, L4391) for 24 hours.

Immunofluorescence Staining

Cells were seeded on coverslips and treated as required. Following treatment, cells were fixed with 4% paraformaldehyde for 10 minutes and permeabilized with 0.2% Triton X-100 for 10 minutes. Subsequently, cells were blocked with 3% bovine serum albumin (BSA; Sigma, SRE0096) for 1 hour at room temperature. The cells were then incubated overnight at 4°C with primary antibodies (diluted to a final concentration of 4 μg/mL in 1% BSA; see Table 1 for catalogue numbers). After washing with PBS, the cells were incubated with appropriate fluorescence-labeled secondary antibodies (1:1000 dilution in 1% BSA; Invitrogen, 488-rabbit: A11008, 594-mouse: A11005) for 1 hour at room temperature in the dark.

Nuclei were counterstained with Hoechst dye (1:5000 dilution in 1% BSA; Invitrogen, H3570) for 5 minutes. Coverslips were mounted using anti-fade mounting medium (Southern Biotech, 0100-01) and imaged using a laser scanning confocal microscope.

Crystal Violet Staining

Five C2C12 cell lines were used for the experiments: OE-ctrl (PLVX), OE (PLVX-*Brip1os*), KD-ctrl (Krab-non), KD-1 (*Brip1os*-g1), and KD-2 (*Brip1os*-g2). Cells were seeded in 12-well plates at a density of 1,000 cells per well and cultured until colony formation. After the designated culture period, the medium was aspirated, and the cells were gently washed once with PBS. The cells were then fixed with 4% paraformaldehyde at room temperature for 10 minutes. Following a PBS wash, they were stained with 0.1% crystal violet solution (Solarbio, G1062) at room temperature for 10 minutes. Excess stain was carefully removed under running tap water. After air-drying at room temperature, images were acquired using a scanner. For quantitative analysis, the stained cells were solubilized with 33% acetic acid, and the absorbance was measured at a wavelength of 570 nm.

CCK-8 Assay

The cell lines used were identical to those in the crystal violet assay. Cells were seeded in 96-well plates at a density of 50 cells per well and treated accordingly after attachment. At predetermined time points, 200 μL of a mixture of CCK-8 solution (APEXBIO, K1018) and complete medium (1:9 ratio) was added to each well. The plate was returned to the incubator for an additional 2 hours. Absorbance was measured at a wavelength of 450 nm using a microplate reader. Wells containing medium without cells were used as blanks for zero adjustment. The optical density (OD) values of the experimental groups directly reflected the number of viable cells.

Flow Cytometry

Briefly, cells were harvested and washed with ice-cold PBS. The cells were resuspended in 100 μL of PBS containing 0.3% BSA and incubated with 1 μL of fluorescence-conjugated antibodies (see Supplementary Table 1 for catalogue numbers) at 4°C in the dark for 40 minutes. After staining, the cells were washed twice with PBS, resuspended in PBS, and analyzed using a flow cytometer. Data acquisition and analysis were performed using CytExpert software.

RNA Sequencing

RNA sequencing and analysis were performed by Epigenome (Guangzhou, China). In brief, total RNA was extracted from samples using the TRIzol method. The RNA was first ligated to 3' and 5' adapters and then reverse-transcribed into cDNA. The resulting cDNA was amplified by PCR, and the target fragment library was size-selected and purified by gel excision. Libraries passing quality control were sequenced on an Illumina platform.

Non-Contact Co-culture

Non-contact co-culture assays were performed using 12-well Transwell plates with a 0.4-μm pore membrane (Corning, 3460).

For the co-culture system with macrophages in the upper chamber and myoblasts in the lower chamber, freshly isolated bone marrow-derived cells were seeded into the Transwell upper chamber at a density of 1×10^5 cells per well and polarized to the M0 or M1 phenotype using the appropriate cytokine stimulation. Subsequently, primary myoblasts, which had been cultured in vitro for 48 hours after isolation, were seeded into the corresponding lower chamber at a density of 5×10^5cells per well. Co-culture was carried out for 6 hours in basal medium devoid of M-CSF or growth factors. The detailed experimental procedures of isolating primary myoblast are described in our previously published protocol [38].

For the co-culture system with myoblasts in the upper chamber and macrophages in the lower chamber, freshly isolated bone marrow-derived primary macrophages were first seeded into the lower chamber at a density of 2×10^5 cells per well and allowed to complete polarization. Following this, primary myoblasts, pre-cultured for 48 hours, trypsinized, and resuspended, were seeded into the Transwell upper chamber at a density of 4×10^4 cells per well. Similarly, co-culture was conducted for 6 hours in basal medium without M-CSF or growth factors.

After the co-culture period, cells from the lower chamber of each well were collected separately for subsequent analyses, including qPCR and flow cytometry. For the detection of MuSCs, the protocol was adapted from a previously described method [39].

Declarations

Acknowledgments

We thank the website https://biogdp.com for providing mechanism diagram materials [40].

Funding

This work was supported by grants from the National Natural Science Foundation of China (82570687, 82425010, 82472770, 82272638), the National Key Research and Development Program of China (2024YFA1107200), the Natural Science Foundation of Guangdong Province (2022A1515011413, 2022A1515010654), the Guangzhou Science and Technology Plan Projects (2024A04J6571, 2024A03J0176, 2025A03J3165, 2024A03J0282, 2023A03J0204), the Cultivation Project for National Natural Science Foundation of China from the Third Affiliated Hospital of Sun Yat-Sen University (2024GZRPYMS01, 2025GZRPYMS01).

Data Availability

All data supporting the findings of this study are available within the paper and its Supplementary Information files.

Ethics approval and consent to participate

This animal study was reviewed and approved by the Institutional Animal Care and Use Committee of Third Affiliated Hospital of Sun Yat-sen University.

Consent to publication

Not applicable.

Competing interests

The authors declare no competing interests.

References

1. Laumonier, T. & Menetrey, J. Muscle injuries and strategies for improving their repair. J. Exp. Orthop. 3, 15 (2016).
2. Bentzinger, C. F., Wang, Y. X. & Rudnicki, M. A. Building Muscle: Molecular Regulation of Myogenesis. Cold Spring Harb. Perspect. Biol. https://doi.org/10.1101/cshperspect.a008342 (2012).
3. Shi, X. & Garry, D. J. Muscle stem cells in development, regeneration, and disease. Genes Dev. 20, 1692–1708 (2006).
4. Kuang, S., Gillespie, M. A. & Rudnicki, M. A. Niche Regulation of Muscle Satellite Cell Self-Renewal and Differentiation. Cell Stem Cell https://doi.org/10.1016/j.stem.2007.12.012 (2008).
5. Fang, J. et al. Redressing the interactions between stem cells and immune system in tissue regeneration. Biol. Direct 16, 18 (2021).
6. De Maria, A., Bozzano, F., Cantoni, C. & Moretta, L. Revisiting human natural killer cell subset function revealed cytolytic CD56dimCD16 + NK cells as rapid producers of abundant IFN-γ on activation. Proc. Natl. Acad. Sci. U. S. A. 108, 728–732 (2011).
7. Panduro, M., Benoist, C. & Mathis, D. Treg cells limit IFN-γ production to control macrophage accrual and phenotype during skeletal muscle regeneration. Proc. Natl. Acad. Sci. U. S. A. 115, E2585–E2593 (2018).
8. Chazaud, B. Inflammation and Skeletal Muscle Regeneration: Leave It to the Macrophages! Trends Immunol. https://doi.org/10.1016/j.it.2020.04.006 (2020).
9. Ivashkiv, L. B. IFNγ: signalling, epigenetics and roles in immunity, metabolism, disease and cancer immunotherapy. Nat. Rev. Immunol. https://doi.org/10.1038/s41577-018-0029-z (2018).
10. Chen, Y.-F., Lee, C.-W., Wu, H.-H., Lin, W.-T. & Lee, O. K. Immunometabolism of macrophages regulates skeletal muscle regeneration. Front. Cell Dev. Biol. 10, 948819 (2022).
11. Martins, L., Gallo, C. C., Honda, T. S. B., Alves, P. T. & Et., A. Skeletal muscle healing by M1-like macrophages produced by transient expression of exogenous GM-CSF. Stem Cell Res. Ther. https://doi.org/10.1186/s13287-020-01992-1 (2020).

12. Toita, R. et al. Collagen patches releasing phosphatidylserine liposomes guide M1-to-M2 macrophage polarization and accelerate simultaneous bone and muscle healing. Acta Biomater. 187, 51–65 (2024).
13. Dort, J., Fabre, P., Molina, T. & Dumont, N. A. Macrophages Are Key Regulators of Stem Cells during Skeletal Muscle Regeneration and Diseases. Stem Cells Int. 2019, 4761427 (2019).
14. Beermann, J., Piccoli, M.-T., Viereck, J. & Thum, T. Non-coding RNAs in Development and Disease: Background, Mechanisms, and Therapeutic Approaches. Physiol. Rev. https://doi.org/10.1152/physrev.00041.2015 (2016).
15. Yao, Y. et al. LncRNA-MEG3 Regulates Muscle Mass and Metabolic Homeostasis by Facilitating SUZ12 Liquid–Liquid Phase Separation. Adv. Sci. 12, 2417715 (2025).
16. Salsi, V. et al. Nucleolar FRG2 lncRNAs inhibit rRNA transcription and cytoplasmic translation, linking FSHD to dysregulation of muscle-specific protein synthesis. Nucleic Acids Res. 53, gkaf643 (2025).
17. Bhatt, B. J. et al. Molecular subtypes of human skeletal muscle in cancer cachexia. Nature 646, 973–982 (2025).
18. Xie, S.-J. et al. Characterization of Long Non-coding RNAs Modified by m6A RNA Methylation in Skeletal Myogenesis. Front. Cell Dev. Biol. 9, (2021).
19. Cheng, M., Nguyen, M.-H., Fantuzzi, G. & Koh, T. J. Endogenous interferon-γ is required for efficient skeletal muscle regeneration. Am. J. Physiol.-Cell Physiol. https://doi.org/10.1152/ajpcell.00568.2007 (2008).
20. Tidball, J. G. Regulation of muscle growth and regeneration by the immune system. Nat. Rev. Immunol. 17, 165–178 (2017).
21. Tan, Y.-Y. et al. Stage-specific requirement for METTL3-dependent m6A epitranscriptomic regulation during myogenesis. Commun. Biol. 8, 1317 (2025).
22. King, M. R. & Colla, S. Muscle Rehabilitation Techniques and Prevention of Injury. Vet. Clin. North Am. Equine Pract. 41, 193–211 (2025).
23. SAKAMOTO, M. Effects of Physical Agents on Muscle Healing with a Focus on Animal Model Research. Phys. Ther. Res. 24, 1–8 (2021).
24. Eming, S. A., Wynn, T. A. & Martin, P. Inflammation and metabolism in tissue repair and regeneration. Science https://doi.org/10.1126/science.aam7928 (2017).
25. Zhang, Y., Wang, T., Wang, Z., Shi, X. & Jin, J. Functions and Therapeutic Potentials of Long Noncoding RNA in Skeletal Muscle Atrophy and Dystrophy. J. Cachexia Sarcopenia Muscle 16, e13747 (2025).
26. Tripathi, G. M. et al. Synaptic-like coupling of macrophages to myofibers regulates muscle repair. Curr. Biol. CB 35, 6010–6023.e5 (2025).
27. Whitaker, R. et al. Effects of injury size on local and systemic immune cell dynamics in volumetric muscle loss. NPJ Regen. Med. 10, 9 (2025).

28. Chi, Z. et al. Gasdermin D-mediated metabolic crosstalk promotes tissue repair. Nature 634, 1168–1177 (2024).
29. Xu, H. et al. Inducible degradation of lncRNA Sros1 promotes IFN-γ-mediated activation of innate immune responses by stabilizing Stat1 mRNA. Nat. Immunol. https://doi.org/10.1038/s41590-019-0542-7 (2019).
30. Wang, Y. et al. Long noncoding RNA derived from CD244 signaling epigenetically controls CD8 + T-cell immune responses in tuberculosis infection. Proc. Natl. Acad. Sci. 112, (2015).
31. Bhatt, B. J. et al. Molecular subtypes of human skeletal muscle in cancer cachexia. Nature 646, 973–982 (2025).
32. Zhang, C. et al. Role of the lncRNA–mRNA network in atherosclerosis using ox-low-density lipoprotein-induced macrophage-derived foam cells. Mol. Omics 16, 543–553 (2020).
33. Lei, S., Chen, R., Shi, H., Zhou, S. & She, Y. lncRNA AK159072 Promotes Myoblast Proliferation and Muscle Regeneration Through Activation of Akt/Foxo1 Pathway. J. Biochem. Mol. Toxicol. 39, e70292 (2025).
34. Wang, Y. et al. lncRNA DLEU2 acts as a miR-181a sponge to regulate SEPP1 and inhibit skeletal muscle differentiation and regeneration. Aging 12, 24033–24056 (2020).
35. Yao, Y. et al. LncRNA-MEG3 Regulates Muscle Mass and Metabolic Homeostasis by Facilitating SUZ12 Liquid–Liquid Phase Separation. Adv. Sci. 12, 2417715 (2025).
36. Jin, K. et al. Targeting the interaction between long noncoding RNA XR_001779380 and Prdm1 to enhance IFN-γ immunity in murine neonatal intestinal epithelial cells. mBio 16, e00773-25 (2025).
37. Kamiya, M. et al. Targeting necroptosis in muscle fibers ameliorates inflammatory myopathies. Nat. Commun. 13, 166 (2022).
38. Luo, Y. et al. Simplifying the protocol for low-pollution-risk, efficient mouse myoblast isolation and differentiation. Adv. Biotechnol. 3, 8 (2025).
39. Liu, L., Cheung, T. H., Charville, G. W. & Rando, T. A. Isolation of skeletal muscle stem cells by fluorescence-activated cell sorting. Nat. Protoc. 10, 1612–1624 (2015).
40. Jiang, S. et al. Generic Diagramming Platform (GDP): a comprehensive database of high-quality biomedical graphics. Nucleic Acids Res. 53, D1670–D1676 (2024).

Figures

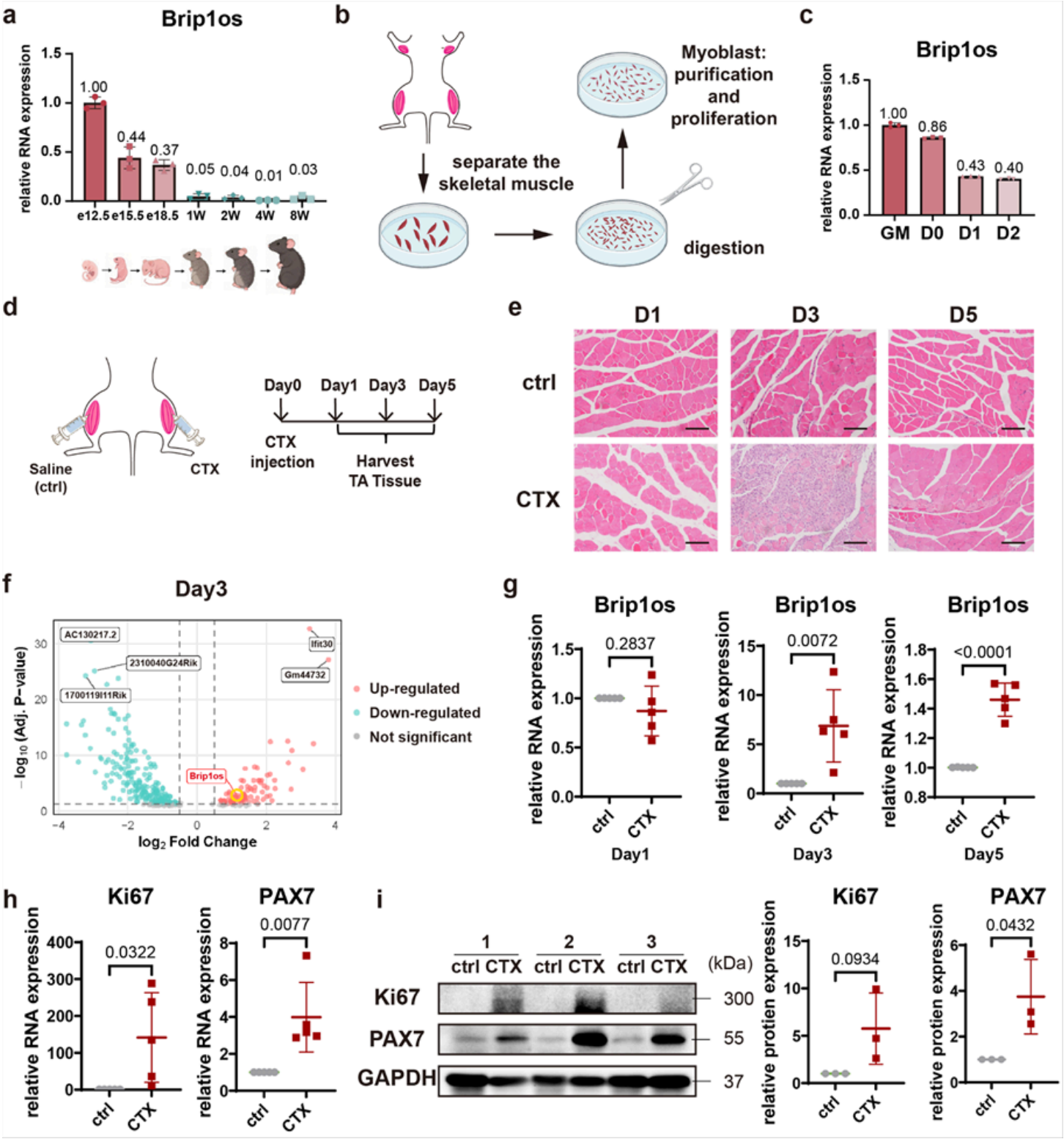


Figure 1

***Brip1os* is involved in muscle development, myoblast differentiation, and early-stage muscle injury repair.**

(a) Expression level of *Brip1os* in mouse muscle tissue during postnatal growth and development. (b) Schematic diagram of the extraction and culture of mouse primary myoblasts. (c) Trend of

*Brip1os*expression during invitro differentiation of primary myoblasts as detected by quantitative PCR (qPCR). (d) Schematic of the cardiotoxin (CTX)-induced tibialis anterior (TA) muscle injury model. CTX was injected into one TA muscle, and phosphate-buffered saline (PBS) was injected into the contralateral side as an internal control. Tissues were collected on days 1, 3, and 5 post-injury for analysis. (e) Representative hematoxylin and eosin (H&E)-stained sections at different time points post-injury, showing the muscle regeneration process. Scale bar, 100 μm. (f-g) RNA sequencing analysis on day 3 post-injury (the point representing *Brip1os* is highlighted in red font and circled in yellow) (f), and qPCR validation of the dynamic expression of *Brip1os* in injured muscle on days 1, 3, and 5(g). (h-i) Expression of Ki67 and PAX7 in muscle on day 3 post-injury as detected by qPCR(h) and western blotting (WB) (i), with protein expression levels quantified by densitometric analysis. (mean ± SD, n = 5)

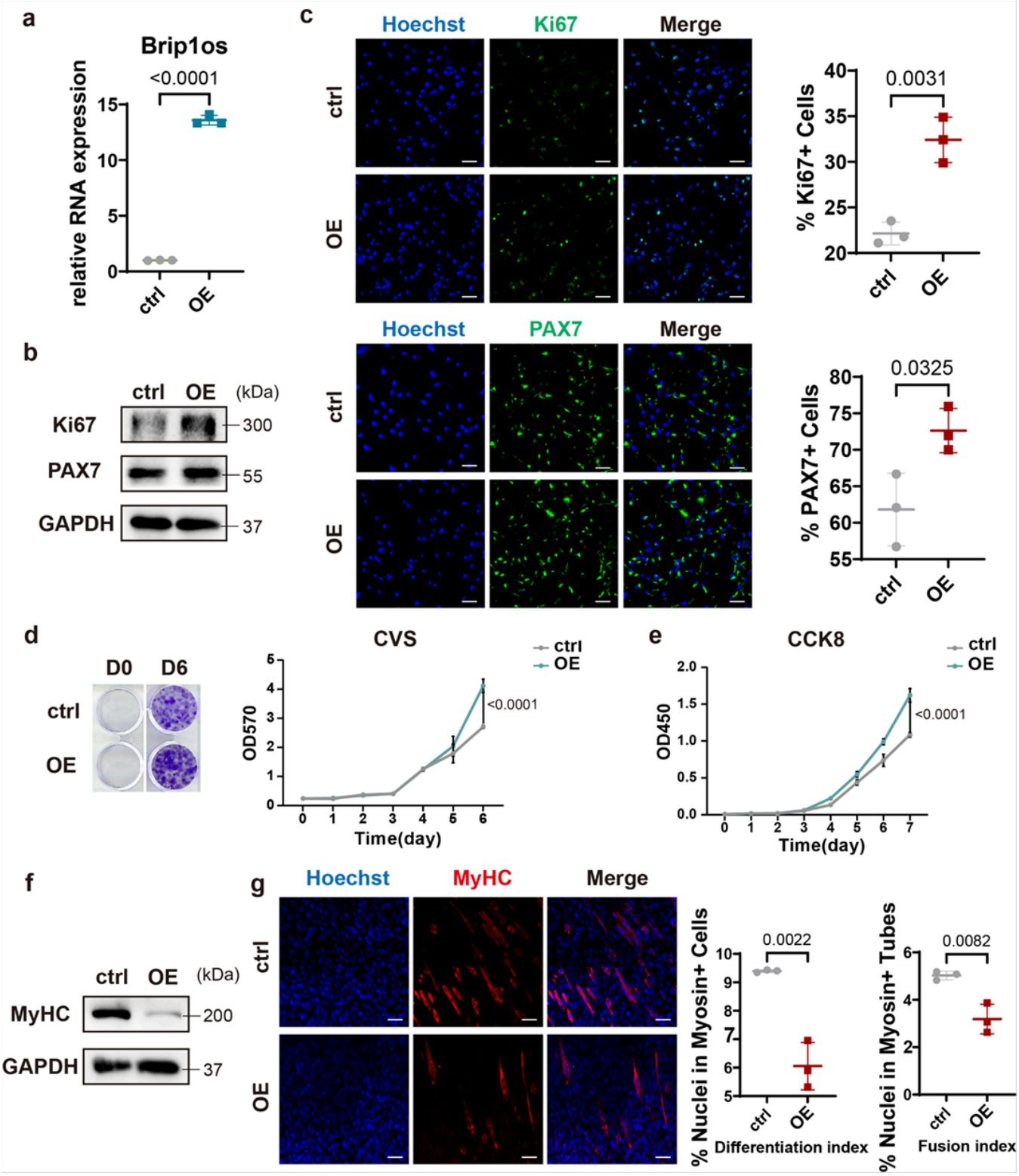


Figure 2

Overexpression of *Brip1os* in C2C12 cells promotes proliferation and inhibits differentiation.

(a) Overexpression efficiency of *Brip1os* in C2C12 cells as detected by qPCR. The overexpression vector used was PLVX-puro. (b) Validation of PAX7 and Ki67 protein levels in growth medium (GM) cells by WB. (c) Representative immunofluorescence (IF) images of PAX7 (green) and Ki67 (green) in proliferating

cells. Nuclei were counterstained with Hoechst (blue). Scale bar, 50 μm. Right: Quantitative statistical analysis of the percentage of PAX7-positive and Ki67-positive cells. (d-e) Cell proliferation and colony formation ability assessed by crystal violet staining (CVS)(d) and CCK-8 assay(e). (f) Validation of myosin heavy chain (MyHC) protein level in differentiating cells on day 3 (D3) by WB. (g) Representative IF images of myosin heavy chain (MyHC, red) in cells on differentiation day 3. Nuclei were counterstained with Hoechst (blue). Scale bar, 100 μm. Right: Quantitative statistical analysis of differentiation index and fusion index. (mean ± SD)

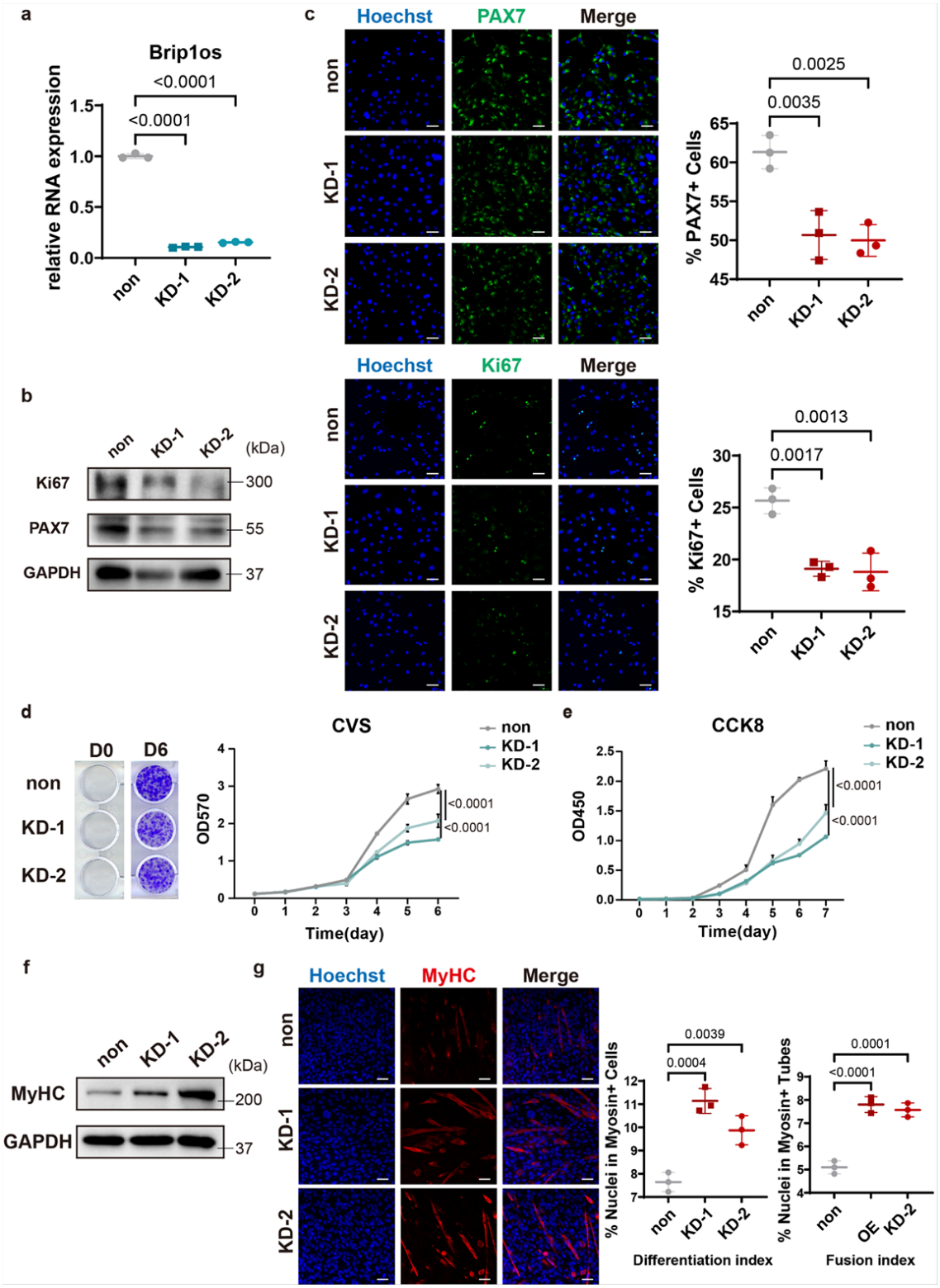


Figure 3

Knockdown of *Brip1os* in C2C12 cells inhibits proliferation and promotes differentiation.

(a) Knockdown efficiency of *Brip1os* in C2C12 cells as verified by qPCR. The vector used was Krab-dCas9. (b) Validation of PAX7 and Ki67 protein levels in growth medium (GM) cells by WB. (c) Representative IF images of PAX7 (green) and Ki67 (green) in proliferating cells. Nuclei were counterstained with Hoechst (blue). Scale bar, 50 μm. Right: Quantitative statistical analysis of the percentage of PAX7-positive and Ki67-positive cells. (d-e) Cell proliferation and colony formation ability assessed by crystal violet staining (CVS) (d) and CCK-8 assay(e). (f) Validation of MyHC protein level in differentiating cells on day 3 (D3) by WB. (g) Representative IF images of MyHC (red) in cells on differentiation day 3. Nuclei were counterstained with Hoechst (blue). Scale bar, 100 μm. Right: Quantitative statistical analysis of differentiation index and fusion index. (mean ± SD)

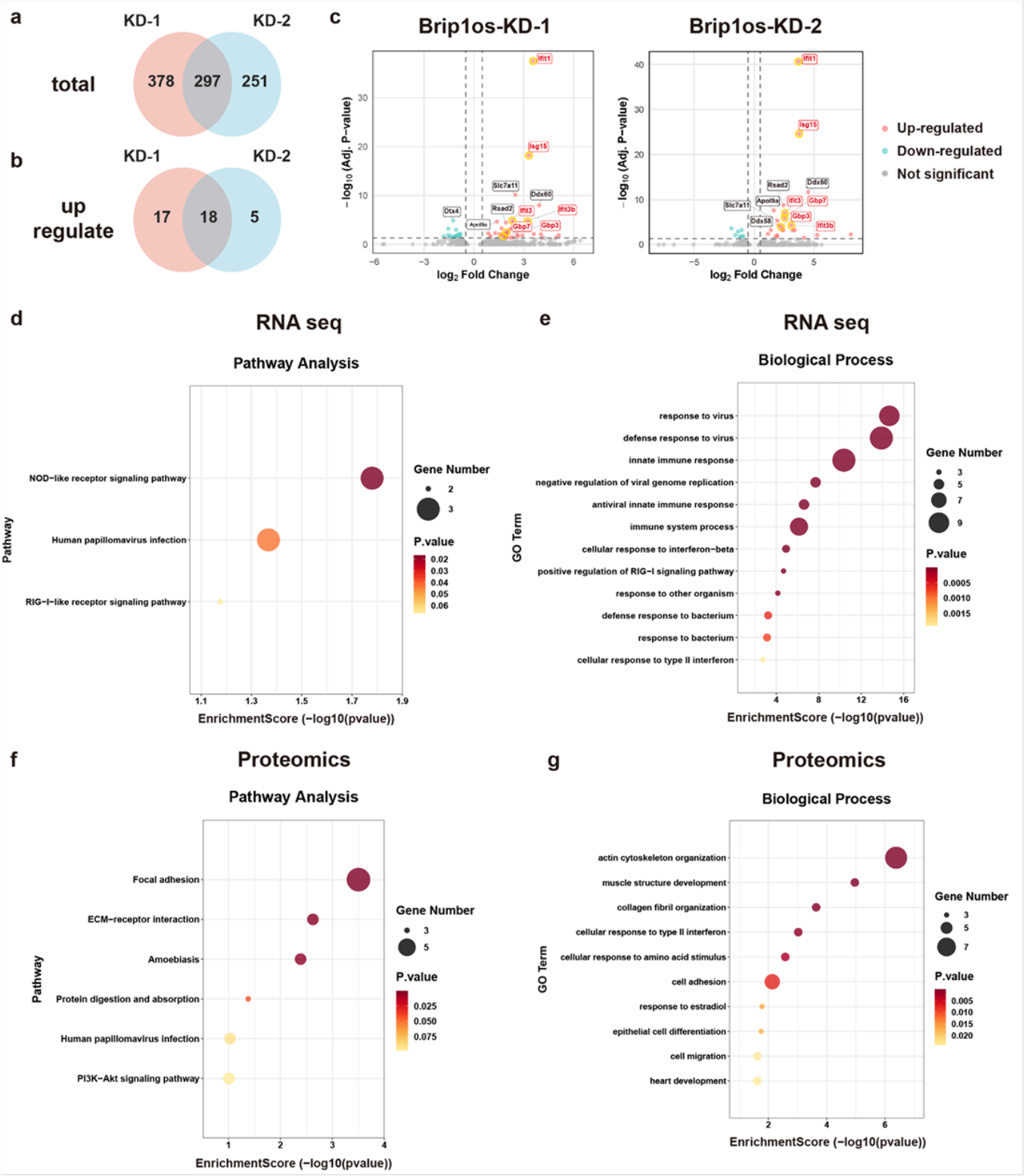


Figure 4

Transcriptomic analysis of C2C12 cells following *Brip1os* knockdown.

(a-b) Venn diagram showing the overlap of significantly upregulated genes in two independent *Brip1os*-knockdown C2C12 cell lines (KD-1 and KD-2). (c) Volcano plot of RNA sequencing results. Genes responsive to interferon-gamma (IFN-γ) are labeled in red font. Besides the target gene, the five most

significantly changed genes are also labeled. (d-e) KEGG pathway enrichment analysis (d) and GO functional enrichment analysis (e) of the differentially expressed genes identified upon *Brip1os* knockdown. (f-g) KEGG pathway enrichment analysis(f) and GO biological process enrichment analysis(g) of differentially expressed proteins in C2C12 cells following *Brip1os* knockdown.

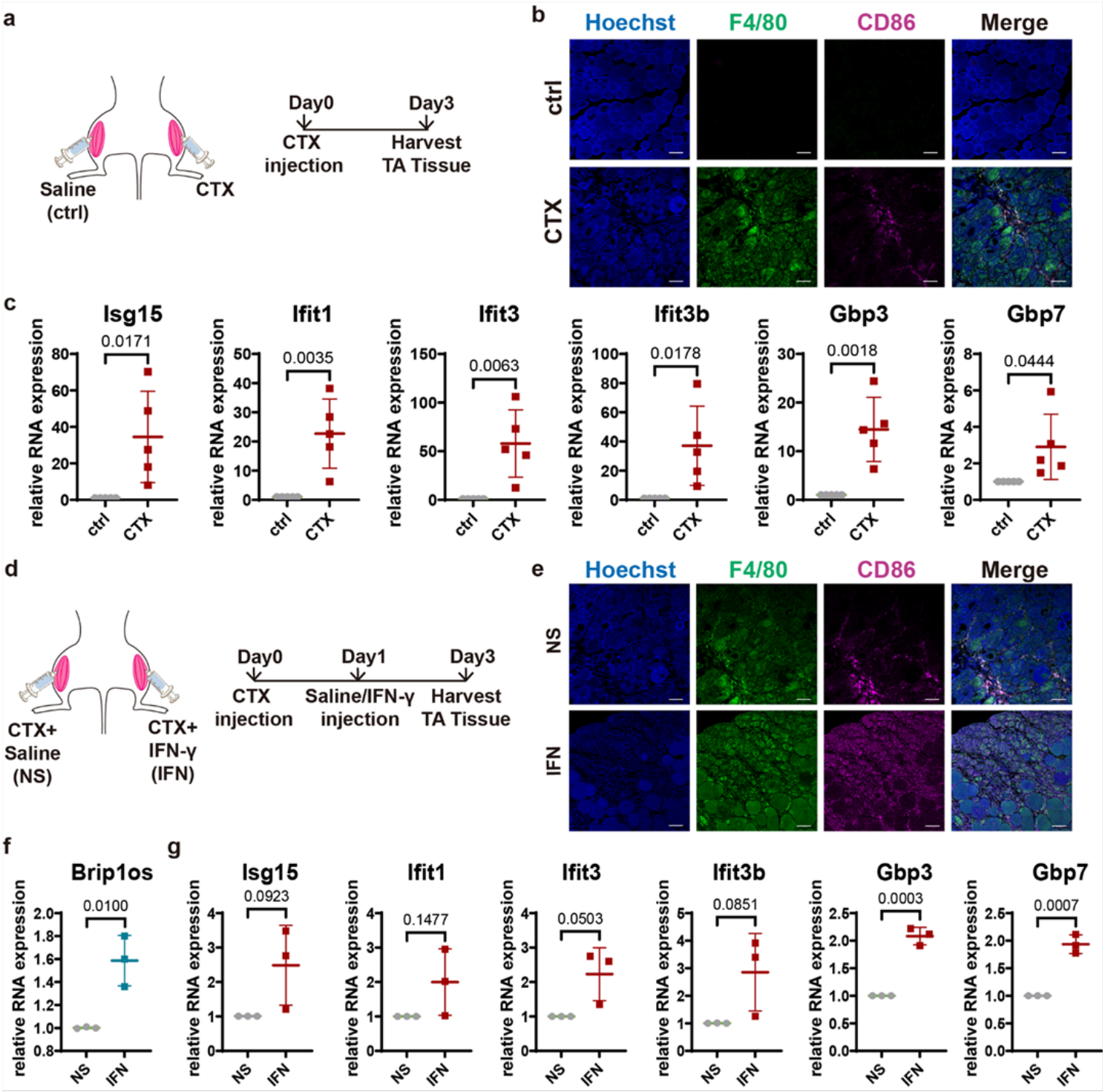


Figure 5

IFN-γ induces M1 macrophage infiltration and downstream gene expression during early muscle injury.

(a-b) Schematic of the CTX-induced TA muscle injury model. Tissues were collected on day 3 post-injury for analysis. M1 Macrophages (F4/80+ CD86+) at the injury site were quantified by IF staining. (c) Expression levels of six IFN-γ-responsive genes in mouse TA muscle on day 3 after CTX injury, compared to the uninjured control, as detected by qPCR. (d-e) Schematic of the combined CTX and IFN-γ treatment experiment. CTX was injected into both TA muscles, with IFN-γ co-injected into one side and PBS into the contralateral side as an internal control. Tissues were collected on day 3 post-injury for analysis. M1 Macrophages (F4/80+ CD86+) at the injury site were quantified by IF staining. (f) Changes in *Brip1os*expression in TA muscle after combined CTX and IFN-γ treatment. (g) Expression levels of six IFN-γ-responsive genes in TA muscle after combined CTX and IFN-γ treatment, compared to the contralateral side injected with CTX and Saline (NS), as detected by qPCR. Scale bar, 50 μm. (mean ± SD, n=5)

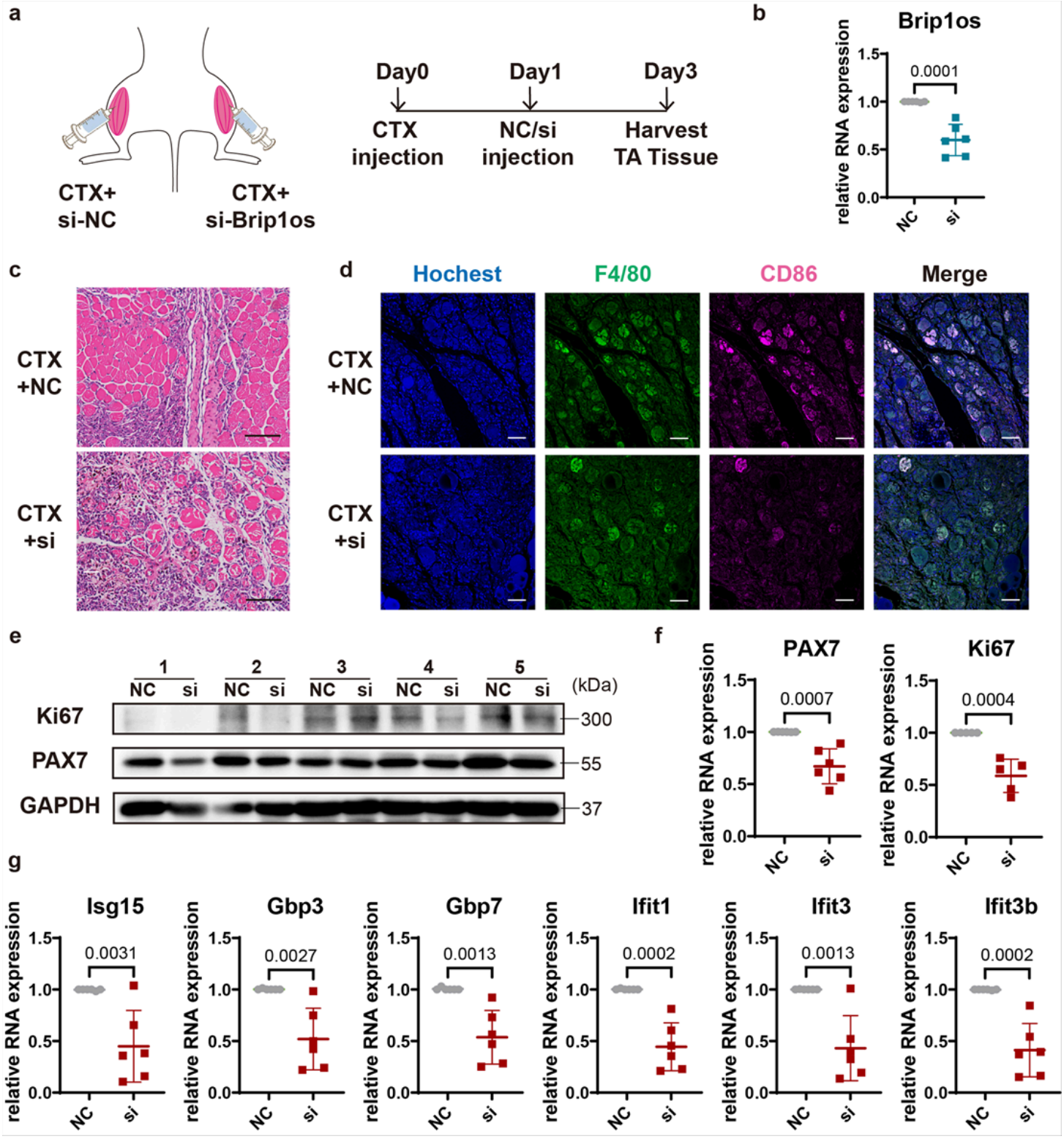


Figure 6

In vivo knockdown of *Brip1os* impairs muscle regeneration and attenuates the early injury response.

(a) Schematic of the experiment involving CTX-induced TA muscle injury combined with local in vivo knockdown of *Brip1os*. (b) Knockdown efficiency of *Brip1os* in injured muscle tissue as verified by qPCR. (c) Representative H&E-stained section images of the contralateral control and *Brip1os*-knockdown TA

muscles on day 3 post-injury. Scale bar, 100 μm. (d) Quantitative analysis of M1 Macrophages (F4/80+ CD86+) at the injury site by IF staining. Scale bar, 50 μm. (e-f) Expression of Ki67 and PAX7 in muscle on day 3 post-injury as detected by qPCR(e) and western blotting (WB) (f). (g) mRNA expression levels of IFN-γ-responsive downstream genes in muscle tissue as detected by qPCR. (mean ± SD, n = 5)

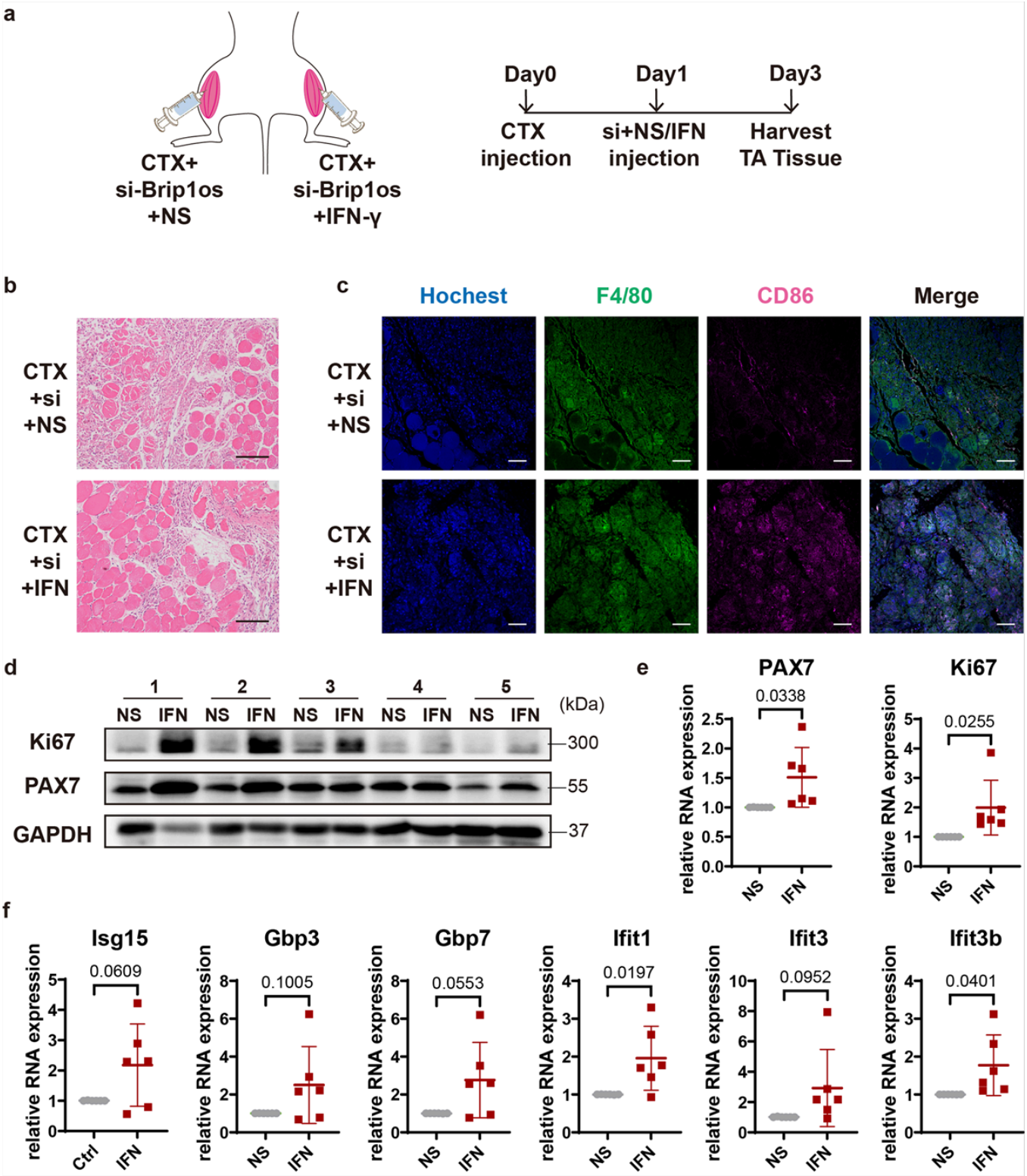
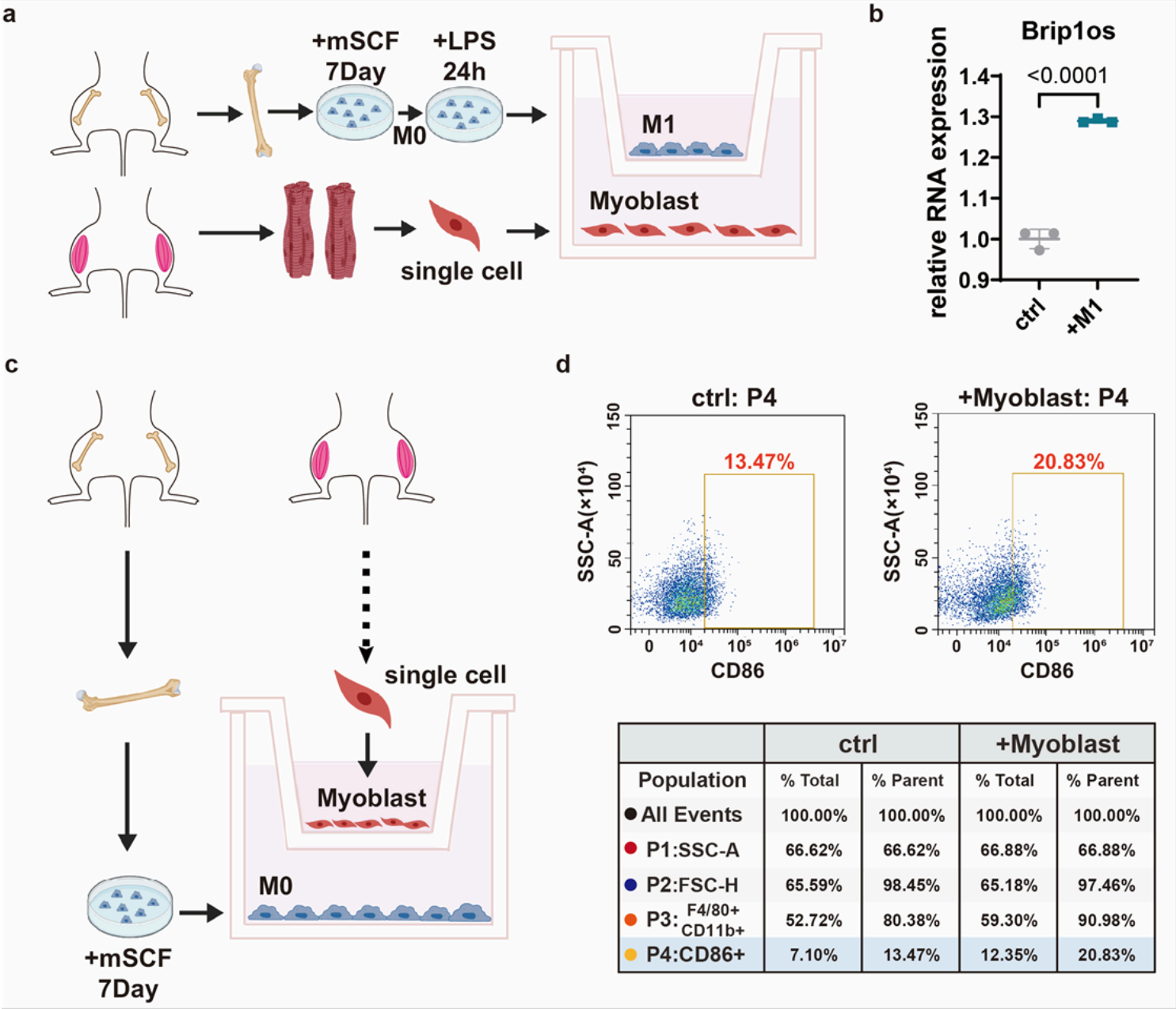


Figure 7

Effect of IFN-γ on muscle regeneration under *Brip1os* knockdown conditions.

(a) Schematic of the experiment involving CTX-induced TA muscle injury, *Brip1os* knockdown, and local supplementation of IFN-γ. (b) Representative H&E-stained section images of the Saline control group and the IFN-γ supplementation group on day 3 post-injury. Scale bar, 100 μm. (c) Quantitative analysis of M1 Macrophages (F4/80+ CD86+) at the injury site in the two groups by IF staining. Scale bar, 50 μm. (d-e) Expression of Ki67 and PAX7 in muscle on day 3 post-injury as detected by qPCR(d) and western blotting (WB) (e). (f) mRNA expression levels of IFN-γ-responsive downstream genes in muscle tissue of the two groups as detected by qPCR. (mean ± SD, n = 5)



	ctrl		+Myoblast	
Population	% Total	% Parent	% Total	% Parent
All Events	100.00%	100.00%	100.00%	100.00%
P1:SSC-A	66.62%	66.62%	66.88%	66.88%
P2:FSC-H	65.59%	98.45%	65.18%	97.46%
P3: F4/80+ CD11b+	52.72%	80.38%	59.30%	90.98%
P4:CD86+	7.10%	13.47%	12.35%	20.83%

Figure 8

***Brip1os* is involved in bidirectional regulation between macrophages and myoblasts.**

(a) Schematic of the non-contact co-culture experiment between M1 Macrophages and primary myoblasts. (b) Expression level of *Brip1os* in primary myoblasts after co-culture with M1 Macrophages, as detected by qPCR. Ctrl group: no cells in the upper chamber; +M1 group: LPS-induced M1 Macrophages were added to the upper chamber. Primary myoblasts in the lower chamber were collected for detection after 6 h of co-culture. (c) Schematic of the non-contact co-culture experiment between primary myoblasts and macrophages. (d) Flow cytometry analysis of the proportion of M1 Macrophages (CD11b+, F4/80+, CD86+) among macrophages after co-culture. Ctrl group: no cells in the upper chamber; +Myoblast group: primary myoblasts cultured for 24 h after extraction were added to the upper chamber. Macrophages in the lower chamber were collected for detection after 6 h of co-culture. (mean ± SD)

Supplementary Files

This is a list of supplementary files associated with this preprint. Click to download.

- AdditionalSupportingInformation.docx
- GraphicalAbstract.tiff
- SupplementaryFigure1.tif
- SupplementaryFigure2.tif
- SupplementaryFigure3.tif
- SupplementaryFigure4.tif
- SupplementaryFigure5.tif
- SupplementaryFigure6.tif
- Originalwesternblots.pdf
- RNAseqData.xlsx